A Technique for Efficiently Modeling Long-Path Propagation for Use in Both FDFD and FDTD

Michael W. Chevalier and Umran S. Inan, *Fellow, IEEE*

***Abstract*—A technique is developed for the efficient modeling of propagation over long paths (hundreds of λ) by breaking the path up into segments and appropriately applying the perfectly matched layer (PML) absorbing boundary condition and the total field/scattered field boundary condition. For finite-difference time-domain (FDTD) simulations the new technique is well suited to model both slow- and fast-wave modes as well as scattering inhomogeneities along the path. In addition, the new technique is directly applicable to finite-difference frequency-domain (FDFD) simulations. Both FDTD and FDFD numerical simulations of propagation within the earth-ionosphere waveguide are performed to validate the new technique.**

***Index Terms*—Finite-difference frequency-domain (FDFD), finite-difference time-domain (FDTD), long-path propagation.**

I. Introduction

MODELING the electromagnetic fields over a long propagation path where the entire path is resolved by a single static grid can be computationally prohibitive (RAM and/or CPU hours) as well as unnecessary. For the case of a transient pulse propagating along a path within a finite-difference time-domain (FDTD) grid, ahead of the transient the fields are zero, and behind the transient the fields are typically zero as well. Much of the fields within the space are, therefore, being unnecessarily computed. The same holds true for the problem of starting up a single frequency transmitter in an FDTD grid. Ahead of the startup transient are zero fields and behind the transient are steady-state fields, both of which are unnecessary to continuously compute. Thevenot *et al.* [1] addressed this problem by developing a moving window technique to reduce the computational domain which captures the moving transient field region along the path. Their motivation was for modeling very low-frequency (VLF) propagation in the earth-ionosphere waveguide. Typically they achieved a grid reduction factor of 10 or so. However, their window size must accommodate all significantly contributing waveguide modes which, in the extreme, can force the window to be as large as the original space. A moving window technique was also developed by [2] at a similar time with similar computational efficiency and accuracy.

In this letter, we develop a technique in which we break up the path into segments. The modeling of VLF propagation in the earth-ionosphere waveguide is used to develop the idea, but the concept is general and can be applied to propagation over any long path. It turns out that any size segment size will naturally accommodate all the forward propagating energy of the waves. This technique is directly applicable to FDTD and FDFD simulations.

Manuscript received July 7, 2006; revised October 10, 2006. This research was sponsored by the Office of Polar Programs of NSF under grant OPP-0093381-001. The collection of the Palmer VLF data was sponsored by the Office of Polar Programs of NSF under grant OPP-0233955.

The authors are with the Space, Telecommunications, and Radioscience Laboratory of the Department of Electrical Engineering at Stanford University, Stanford, CA 94305 USA (e-mail: chamonix@stanford.edu; timothyc@stanford.edu; inan@nova.stanford.edu).

Digital Object Identifier 10.1109/LAWP.2006.887551

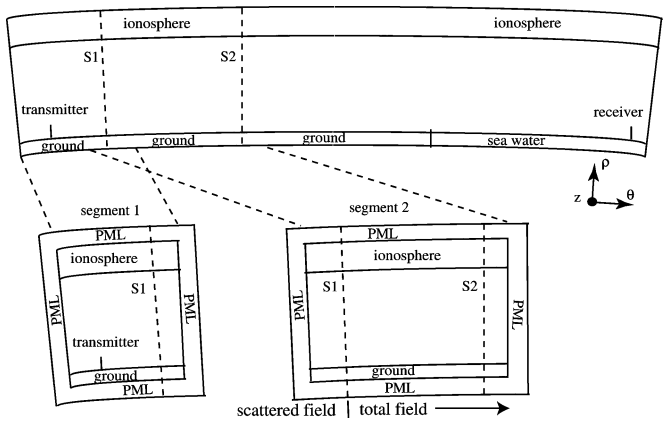

Fig. 1. Earth-ionosphere waveguide. Segments 1 and 2 represent sequential finite-difference spaces that are solved to calculate the electromagnetic fields from the transmitter to the receiver. The fields from surface "S_1" are saved from segment 1 and used as input fields to segment 2. The fields from surface "S_2" would then be used for segment 3 (not shown), etc.

II. A Segmented Long-Path Propagation Technique

Fig. 1 represents a two-dimensional (2-D) space where there exists a transmitter on one end and a receiver on the other. We will assume the space to be 200×5000 cells, where our cell size is 500 m. For this particular space, the ionosphere and the ground act as a waveguide for frequencies in the VLF range ($\sim$20 kHz) and is known as the earth-ionosphere waveguide. If we apply the FDTD technique to this space it could take more than 15 000 timesteps for all the energy of a transient pulse, originating at the transmitter, to pass through the space. Due to higher order waveguide modes it could take a similar amount of time for the space to reach steady state from the transient startup of the transmitter radiating at a single frequency in FDTD. Also for the single-frequency case, we could apply the FDFD technique, which requires an implicit solve, whose matrix solution require hundreds of gigabytes of RAM for a fast direct solver or up to tens of gigabytes of RAM for slower iterative solvers that require preconditioning matrices to condition the system. Due to resource constraints, either RAM and/or time it would be beneficial not to have to solve the whole space at once.

In order to overcome these problems, we break up the space into overlapping segments, an example of which is shown in

segment 1 and segment 2 from Fig. 1. Each segment is surrounded with the perfectly matched layer (PML) boundary condition [3]–[5] to absorb outgoing waves. The idea here is to solve the fields radiated from the transmitter in segment 1 while saving the fields over the surface labeled "S_1"; over time for FDTD, and for FDFD, the complex fields. These fields would be saved in a file on the hard disk, not in RAM. Segment 2 overlaps segment 1 such that "S_1" represents the same region in space. The fields from surface 'S_1' in segment 1 then become the input source fields on the surface "S_1" in segment 2. Now in segment 2, to the right of the input source fields at "S_1," we calculate the total field while to the left we calculate only the scattered fields. The surface at "S_1" in segment 2 is known as a total field/scattered boundary [6]. This formulation is adapted so that any backscatter due to spatial changes in the ionospheric and/or ground parameters within the local segment are absorbed by the PML in the scattered field region. Then we calculate the fields within segment 2 using the input source fields at "S_1" and save the output fields at "S_2." This process is repeated for all subsequent segments until the receiver. We call this the "segmented long path" (SLP) technique.

By breaking our space up into segments we are neglecting interactions between scattering regions from different segments. Also, because of this, a scattering region should be entirely contained within a segment so that the scattering is entirely solved for within the segment. By scattering region, we mean anything the causes backscatter, e.g., inhomogeneities in material or terrain, etc. The segments along the path can all be differing lengths. In this letter we perform FDFD and pulsed FDTD simulations. To reiterate, for the FDFD SLP runs, the general algorithms are as follows.

1) Solve fields in segment N. In segment N, save the electric and magnetic fields and currents over the surface "S_N." At segment $N+1$ apply these fields as the incident fields at the total-field/scattered-field boundary.
2) $N = N + 1$. Go to 1).

Likewise, for the pulsed FDTD SLP runs, the general algorithm is as follows.

1) Solve fields over time in segment N. In segment N, when the fields at "S_N" exceed some threshold (set by user) save the electric and magnetic fields and currents over the surface 'S_N' (in a file on hard disk) over the remaining duration of the run. At segment $N+1$ apply these fields (from file) as the incident fields at the total-field/scattered-field boundary.
2) $N = N + 1$. Go to 1).

These are general algorithms independent of the order and type of the finite-difference methods being applied. To properly solve the particular finite-difference equations at the total-field/scattered field boundary at the surface "S_N" in segment "$N+1$," then in the prior segment "N," at surface "S_N" one must save all the fields necessary to fully specify the incident fields, i.e., the full stencil of the incident fields that will satisfy the finite difference equations at the total-field/scattered-field boundary in segment "$N+1$." This requires one to save the fields at surface "S_N" over a volume of space which encompasses the cross section of the space and typically a few cells of thickness along the path direction (e.g., two cells for second-order spatial differencing, four cells for fourth-order spatial differencing, etc).

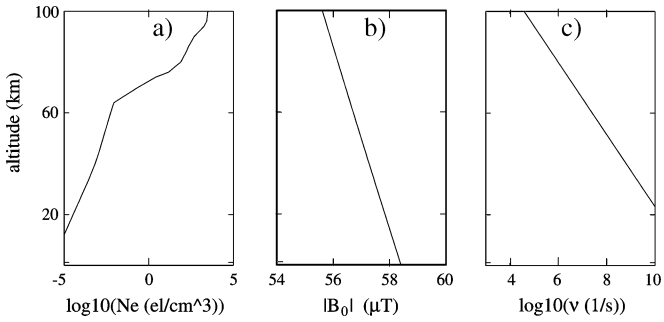

Fig. 2. Ionospheric parameters used to model the earth-ionosphere waveguide. a) Electron density versus altitude. b) Ambient magnetic field versus altitude. c) Electron collision frequency versus altitude.

Each segment because there is overlap between segments has extra RAM overhead proportional to the total length, in cells, of the overlap regions, L_{overlap}. For cases in this letter $L_{\text{overlap}} = 40$ cells. For our larger numerical tests, we will have each segment be 1000 cells long, thus, the percentage of extra RAM from overlap is typically small.

III. Numerical Results and Discussion

We now present some numerical simulations of the SLP technique for both FDTD and FDFD applied to the same waveguide. Our space consists of a 2-D grid in cylindrical coordinates which takes into account the curvature of the earth from the transmitter to the receiver as depicted in Fig. 1. The ionosphere is modeled as a cold magnetized collisional electron plasma. The input parameters into the magnetized plasma equations are electron density, N_e, static magnetic field, $\vec{B}_0$, and collision frequency, ν, all of which are functions of altitude, examples of which used in the modeling are plotted in Fig. 2. To note, in the simulations presented the direction of $\vec{B}_0$ is about 12° w.r.t the ρ axis in the $\rho\theta$ plane. The specific profiles we use are that of an ambient nighttime mid-latitude ionosphere from [7] where the reflection height of 20 kHz radio waves are typically in the range of 80–90 km. The magnetized plasma equations of the ionosphere are implemented in FDTD using (9) from [8] and for FDFD using (6) from [8]. However, our grid implementation is slightly different only in that the cited authors located their vector electric currents, $\vec{J}$ at the grid nodes while we colocate each vector electric current component with its corresponding vector electric field component, e.g., $\vec{E}_x$ and $\vec{J}_x$ are collocated, etc. For the ground we assume $\epsilon_r = 10.0$, $\sigma = 10^{-3}$ S/m, and sea water we assume, $\epsilon_r = 81.0$, $\sigma = 4.0$ S/m, where ϵ_r is the relative permitivity and σ is the electrical conductivity. The transmitter is a short electric monopole pointed in the $\hat{\rho}$-direction located 1 km above the ground. We model the numerical space with approximately 500 m cells to properly sample the free space wavelength of a 19.4 kHz wave with about 30 cells. All PMLs used are 10 cells thick. All FDTD simulations were run at 0.7 of the courant condition.

Two tests were run on both the FDFD and FDTD techniques. In test 1, we model the space from Fig. 1 along the first 500 km of the path. For run 1 of test 1, we model the entire 500

km in a single grid. For run 2 of test 1, we apply the SLP technique using the following sequence L of segment lengths in kilometers where $L = (100\,100\,100\,100\,100\,100)$. Each successive segment overlaps the prior segment for 20 km, i.e., the total/scattered boundary occurs at 10 km into the space and the fields saved near the end of the segment at surface "S_N" occurs at 10 km before the end of the space. The SLP technique requires six segments. We ran test 1, first applying the FDFD technique at 19.4 kHz, extracting the ρ-directed electric fields along the ground and then plotting the amplitude of E_ρ and E_θ versus distance. The results are plotted in Fig. 3(a) and show excellent agreement. Fig. 3(b) zooms in on the E_θ field plot to display the slight error due to the SLP technique. For the FDTD technique, at the source we radiate a modulated gaussian pulse centered at 19.4 kHz with a 10 kHz bandwidth. For run 1, the FDTD simulation was run for 5000 timesteps. For run 2a, the SLP simulation used the following sequence T of timesteps where T =(3500,3500,3500,3500,3500,3500) and T_i, the ith timestep entry, corresponds to the amount of timesteps that the ith segment runs for. For FDTD, in addition to the RAM savings, we can calculate percentage savings of CPU hours for the SLP technique relative to the full grid technique. This is given by the formula

$$\text{percentage of CPU hour savings} = \left(1 - \frac{\Sigma_i T_i L_i}{T_f L_f}\right) \times 100 \quad (1)$$

where T_i is the number of timesteps run in the ith segment and L_i is the length of the ith segment. L_f is the full grid length (in kilometers) and T_f is the number of timesteps that the full grid ran. The CPU hour savings, applying (1), is about 14%. For run 2b, the SLP simulation used the following sequence T of timesteps where T = (1500,1500,1750,2000,2250,2500). The number of timesteps for each successive segment is increased to account for the dispersion of the fields. The CPU hour savings, applying (1), is about 54%. Fig. 3(c) and (d) plot E_ρ and E_z over time, respectively, just above the ground at a distance of 480 km along the path. In Fig. 3(c), the agreement is very good for all runs. Fig. 3(d) is more interesting, the field levels are smaller and we see the train of pulses for the different waveguide modes. For run 2a, the agreement is again excellent with run 1 for the entire duration. For run 2b, which ends at about 4100 timesteps, the results capture up to just past the fourth train pulse. One sees error in run 2a beginning near timestep 3400. Fig. 3(e) shows a zoom in of the E_z field to better illustrate the error that run 2b of the SLP technique introduces. The solution of run 2b rings about the solutions of run 1 and run 2a. To explain this error, we notice that for both run 2a and run 2b the input fields into each segment are truncated in time when they are saved from the prior segment. The FDTD spaces are then run past the truncation, in time, of the input source fields. This is a discontinuity in the source fields which can then propagate through the space. The sequence of timesteps for run 2a is such that these "discontinuity" fields, say in segment "N," never reach the surface "S_N" of segment "N" and, therefore, are not saved as input fields into the next segment. However, for run 2b, the sequence of timesteps are successively increasing in the number of timesteps and the "discontinuity" fields do reach surface "S_N" of segment "N" to be saved as input fields, thereby

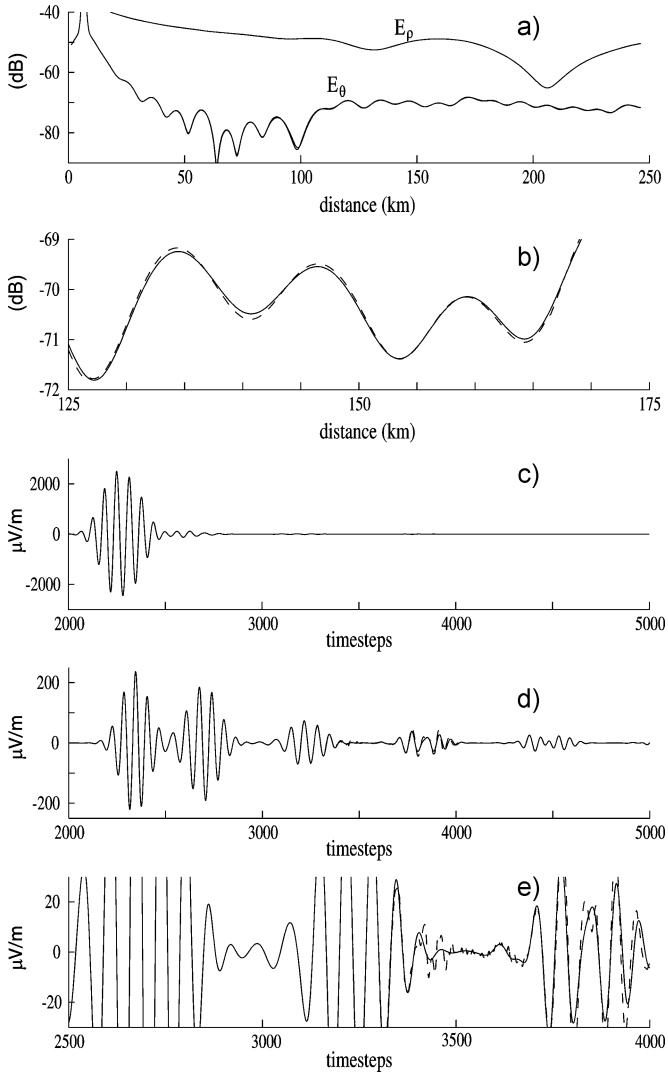

Fig. 3. Test 1 results (all plots: full grid-solid line, SLP—dashed line). a) FDFD plots of E_ρ and E_θ just above ground versus distance. b) FDFD plot: zoom in of E_θ. c)–e) to the resolution of the plot, results from run 1 match results from run 2a. c) FDTD plot of time domain pulse of E_ρ just above ground at 480 km distance. d) FDTD plot of time domain pulse of E_z just above ground at 480 km distance. e) FDTD plot: zoom in of E_z.

propagating through succeeding segments. Even though run 2b introduces nonphysical waves into the system, it still matches run 1 and run 2a until timestep 3400 and reasonably captures the pulse up to timestep 4000. One possible fix for this truncation error might be to decay the source fields, say starting 100 timesteps before the truncation, to reduce the effects of this discontinuity. However, that is a topic of current research and is not explored in this letter.

For test 2, we model the entire space in Fig. 1, which is about 2500 km in length. For the SLP technique, the sequence of segment lengths L in kilometers are L = (100 500 500 500 500 500), 6 segments in all, with 20 km overlap as in test 1. For FDFD, our resources only allow us to run up to 500 km segments. We therefore must apply the SLP technique. The results are plotted in Fig. 4(a) for only the SLP technique. Based on the excellent agreement between the standard FDFD and the SLP technique from test 1, we expect these results to be accurate. For FDTD, in run 1 we run the

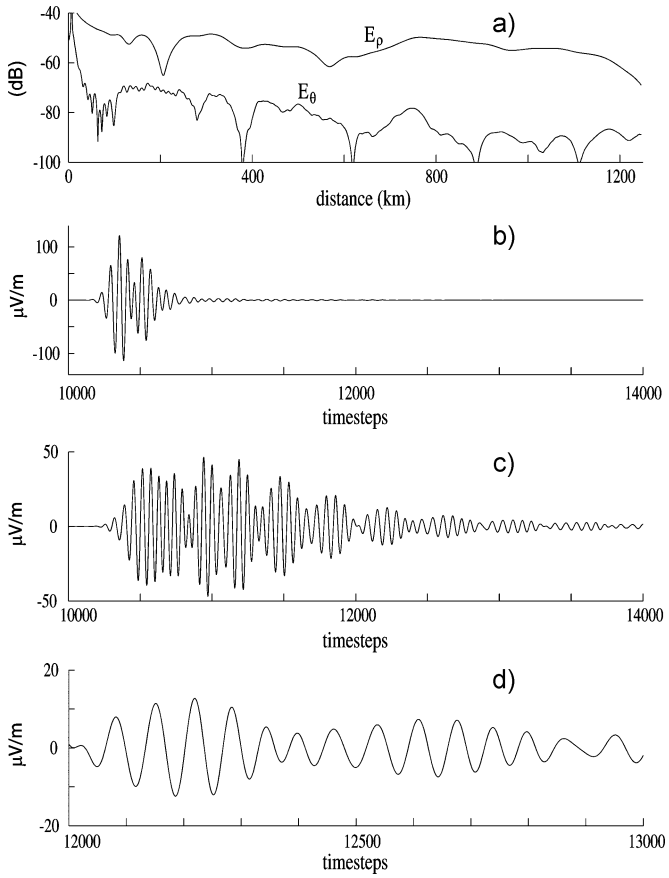

Fig. 4. Test 2 results (all plots: full grid-solid line, SLP—dashed line). a) FDFD plots of E_ρ and E_θ just above ground versus distance (full grid solution not computed due to unavailable resources). b) FDTD plot of time domain pulse of E_ρ just above ground at 2480 km distance. c) FDTD plot of time domain pulse of E_z just above ground at 2480 km distance. d) FDTD plot: zoom in of E_z.

entire grid for 14 000 timesteps. For run 2, the SLP simulation used the following sequence T of timesteps where $T =$ (8000,8000,8000,8000,8000,8000) and T_i, the ith timestep entry, corresponds to the amount of timesteps that ith segment runs for. The CPU hour savings, applying (1), is about 40%. Fig. 4(b) and (4c) plot E_ρ and E_z over time, respectively, just above the ground at a distance of 2480 km along the path. Fig. 4(d) zooms in on E_z. As expected the SLP technique, to the plot resolution, matches with the full grid solution.

For the SLP tests, close examination of all of our calculations in this letter indicates that the backscattered fields are always negligible in magnitude (typically smaller by a factor of $>$50 dB) compared to the forward propagating fields. This is primarily because other than the ground-to-sea transition (1 cell transition) in the waveguide no scattering objects, e.g., regions of ionospheric conductivity change, were placed along the path as to study the SLP technique modeling scattering effects. The numerical results above were more to validate the SLP technique along a homogeneous ionospheric path. But, as mentioned before, based on purely theoretical arguments, by breaking our space up into segments we are neglecting interactions between scattering regions from different segments. Because of this, a scattering region should be entirely contained within a segment so that the scattering is entirely solved for within the segment.

In FDTD, the SLP technique as it relates to the moving-window technique requires more computation. This is because the moving window technique moves with the pulse, and the SLP technique requires the pulse to pass through each segment. However, the SLP technique is more versatile. It is capable of capturing up to the entire dispersion of the pulse where a static sized moving-window, in general, cannot. Especially in waveguides, where the dispersion can be very large, the SLP is better suited. Also, for the SLP technique the segments size and the number of timesteps run for each segment can be varied throughout the space. For FDFD one cannot apply the moving window techniques since it is specifically for the time-domain. The SLP technique is the only option and does very well.

IV. Summary

In this letter, we have developed a new technique, called the SLP technique, for efficiently modeling long propagation paths for use in both FDFD and FDTD. For FDTD, the SLP technique is well suited for capturing both fast and slow modes while providing both RAM and CPU hour savings. For FDFD, the SLP technique, to the authors knowledge, is currently the only method for efficiently solving long paths. Applying the SLP technique to model multiple scattering regions along the path was discussed, theoretically, but was not numerically tested and is a topic of current research. Further applications of the SLP technique are being investigated such as applying the method to long path propagation within periodic structures.

References

[1] M. Thevenot, J. P. Berenger, T. Monediere, and F. Jecko, "A FDTD scheme for the computation of VLF-LF propagation in the anisotropic earth-ionosphere waveguide," *Ann. Telecommun.*, vol. 54, pp. 297–310, 1999.

[2] F. Akleman and L. Sevgi, "A novel finite-difference time-domain wave propagator," *IEEE Trans. Antennas Propagat.*, vol. AP-48, no. 5, pp. 839–841, May 2000.

[3] J. P. Berenger, "A perfectly matched layer for the absorption of electromagnetic waves," *J. Comput. Phys.*, vol. 114, pp. 185–200, 1994.

[4] W. C. Chew and W. H. Weedon, "A 3-D perfectly matched medium fom modified Maxwell's equations with stretched coordinates," *Microw. Opt. Tech. Lett.*, vol. 7, no. 13, pp. 599–604, Sept. 1994.

[5] M. W. Chevalier and U. S. Inan, "A PML using a convolutional curl operator and a numerical reflection coefficient for general linear media," *IEEE Trans. Antennas Propagat.*, vol. 2, no. 7, pp. 1647–1657, Jul. 2004.

[6] A. Taflove and S. C. Hagness, *Computational Electrodynamics: The Finite-Difference Time-Domain Method*, 2nd ed. Norwood, MA: Artech House, 2000.

[7] M. P. Johnson, U. S. Inan, and D. S. Lauben, "Subionospheric vlf signatures of oblique (nonducted) whistler-induced precipitation," *Geophys. Res. Lett.*, vol. 26, p. 3569, 1999.

[8] J. H. Lee and D. K. Kalluri, "Three-dimensional FDTD simulation of electromagnetic wave transformation in a dynamic inhomogeneous magnetized plasma," *IEEE Trans. Antennas Propagat.*, vol. 47, no. 7, pp. 1146–1151, Sep. 1999.